PCCP

ROYAL SOCIETY OF CHEMISTRY

PAPER

View Article Online
View Journal | View Issue

Cite this: *Phys. Chem. Chem. Phys.*, 2023, **25**, 13004

Photodissociation of bromine-substituted nitroimidazole radiosensitizers†

Lassi Pihlava, *[a] Marta Berholts, [b] Johannes Niskanen, [a] Anton Vladyka, [a] Kuno Kooser, [b] Christian Stråhlman, [c] Per Eng-Johnsson, [d] Antti Kivimäki [e] and Edwin Kukk[af]

Received 19th October 2022,
Accepted 23rd April 2023

DOI: 10.1039/d2cp04888d

rsc.li/pccp

Heavy elements and some nitroimidazoles both exhibit radiosensitizing properties through different mechanisms. In an effort to see how the overall radiosensitivity might be affected when the two radiosensitizers are combined in the same molecule, we studied the gas-phase photodissociation of two brominated nitroimidazoles and a bromine-free reference sample. Synchrotron radiation was employed to initiate the photodynamics and energy-resolved multiparticle coincidence spectroscopy was used to study the ensuing dissociation. We observed the brominated samples releasing high amounts of potentially radiosensitizing fragments upon dissociation. Since bromination also increases the likelihood of the drug molecule being ionised per a given X-ray dose, we conclude that heavy-element substitution of nitroimidazoles appears to be a viable path towards new, potent radiosensitizer drugs.

1 Introduction

Ionising radiation (either photons or particles) is used in radiotherapy to damage cancerous cells. While radiotherapy targets tumour cells, some damage is inevitably inflicted on neighbouring healthy cells. This collateral damage is an unwanted side effect, partial elimination of which is possible by improving the selectivity towards malignant cells during the radiation treatment. This can be achieved by using radiosensitizers, agents that increase the effectiveness of radiotherapy.[1–4]

Oxygen mimetics, such as some nitroimidazoles (Fig. 1 shows the nitroimidazole molecules that are studied here), are compounds with high electron affinity that imitate the role of oxygen in the radiosensitization process.[3] Oxygen is a well-known radiosensitizer, which promotes the infliction of irreparable DNA damage *via* formation of peroxide.[2] In the absence of oxygen, peroxide formation is suppressed and damaged DNA is more readily repaired. Solid tumours are often hypoxic, oxygen depleted, and consequently more radioresistant than well-oxygenated tumours. Re-oxygenating hypoxic cells is challenging due to insufficient tumour angiogenesis and constant use of oxygen in cellular respiration. Oxygen mimetics on the other hand may penetrate the tumour further than oxygen, proving valuable in hypoxia-targeted radiotherapy. Dissociation dynamics of various nitroimidazole compounds have been studied actively in recent years,[5–11] and special attention has been given to release of radicals and fragments related to the nitro group. In particular, neutral NO radicals have strongly been associated with radiosensitization.[12]

Heavy elements can have a radiosensitizing effect mainly *via* three mechanisms.[1] First, heavy elements have a higher X-ray absorption cross section than light elements and therefore act as absorption hotspots. Heavy element substitution into a drug molecule would consequently increase the density of the

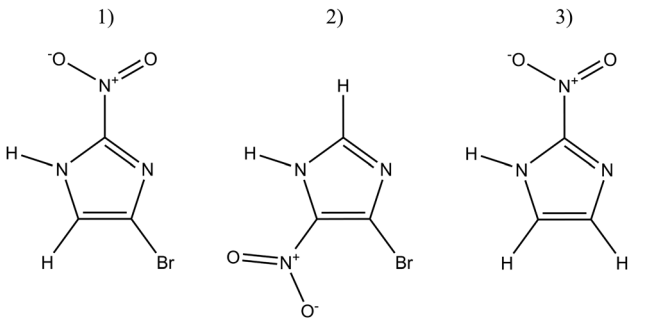

Fig. 1 Structural formulae of the investigated molecules: (1) 4-bromo-2-nitroimidazole (4Br2NIM), (2) 4-bromo-5-nitroimidazole (4Br5NIM), and (3) 2-nitroimidazole (2NIM).

[a] *Department of Physics and Astronomy, University of Turku, FI-20014 Turku, Finland. E-mail: leapih@utu.fi*
[b] *Institute of Physics, University of Tartu, EE-50411 Tartu, Estonia*
[c] *Department of Materials Science and Applied Mathematics, Malmö University, SE-20506 Malmö, Sweden*
[d] *Department of Physics, Lund University, SE-20100 Lund, Sweden*
[e] *MAX IV Laboratory, Lund University, SE-20100 Lund, Sweden*
[f] *Laboratoire de Chimie Physique-Matière et Rayonnement, UMR 7614, CNRS, Sorbonne University, FR-75005 Paris, France*

† Electronic supplementary information (ESI) available. See DOI: https://doi.org/10.1039/d2cp04888d

molecules that dissociate and release radicals into cancerous cells, under a given X-ray dose and drug concentration. Second, core ionisation of heavy atoms may lead to an Auger cascade. Ejected electrons only travel a short distance before stopping, thus resulting in a localised energy deposition (*i.e.* absorbed dose) in a small volume around the emitter. Third, in addition to emission of more secondary electrons, heavy element substitution also increases the likelihood that drug molecules are ionised by electrons due to an increased electron impact ionisation cross section. These factors will be considered in more detail in Section 3. In addition to heavy element substituted organic molecules, a lot of radiosensitization research is centered around nanomaterials incorporating heavy element atoms. Noble metal (silver, platinum, gold) nanomaterials have particularly shown great promise.[1,3,4]

A promising *in vitro* study showed that iodinated nitroimidazole radiosensitizers performed better with hypoxic cells than their iodine-free counterparts.[13] Thus, further research on halogenated nitroimidazoles could lead to more potent radiosensitizers. Studies of the fragmentation of isolated radiosensitizer molecules greatly simplify interpretations one can make about sensitization mechanisms relying on fundamental physics, in stark contrast to clinical trials, where it is impossible to track all the processes the radiosensitizer undergoes during radiotherapy. When considering possible clinical applications, however, there are additional factors that are beyond the scope of *in vacuo* studies, such as biostability, toxicity and tolerability. For example misonidazole, a potent radiosensitizing nitroimidazole, turned out to be a neurotoxin and at clinically tolerable doses its radiosensitizing effect was small.[2,14]

Thus far the study of halogen-containing radiosensitizers has mostly centered around halopyrimidines and halonucleobases (see *e.g.* ref. 15–19). We investigate the prospect of combining a nitroimidazole with a heavy element (bromine) atom. Halogen atoms are especially intriguing heavy element candidates, given the link between high electron affinity and oxygen mimetic's efficacy. Additionally, nitroimidazoles contain hydrogen atoms making halogenation a logical course of action. Samples 4-bromo-2-nitroimidazole, 4-bromo-5-nitroimidazole, and 2-nitroimidazole (henceforth referred to as 4Br2NIM, 4Br5NIM, and 2NIM, respectively) were studied utilising multiparticle coincidence spectroscopy and soft X-ray ionisation. Our experimental design enables simultaneously studying the effects of bromination, the position of the nitro group and the location of the initial ionisation site on the photodissociation dynamics. The possible environmental effects on the photodissociation dynamics posed by the surrounding water molecules in a cellular setting are naturally absent in our *in vacuo* experiment. Future studies on, for example, water clusters doped with BrNIM or other similar compounds would be a natural extension of the present study and would shed light on the environmental effects.

In terms of specificity of the site of the initial ionization, we targeted the atomic N 1s, C 1s and Br 3d core orbitals. The photon energies used in radiotherapy are much higher than here, but the study will nonetheless shed light on relevant core-ionisation dynamics. Hard X-rays primarily ionise deeper halogen orbitals and these core-excited states likely decay *via* X-ray fluorescence, which may transfer some holes to the orbitals studied here. In addition to photoelectric effect, ionisation also happens *via* Compton scattering and electron collisions. Furthermore, since X-ray-induced and electron-impact-induced molecular fragmentation patterns bear many similarities, the study is also relevant in terms of the radiosensitizing effects prompted by secondary ionisations.

2 Experimental setup

The experiment was performed at the gas-phase endstation[20] of the FinEstBeAMS beamline[21,22] of the MAX IV synchrotron radiation facility. The beamline receives radiation from an APPLE II type undulator and is equipped with a plane grating monochromator (SX700 type, FMB Feinwerk-und Messtechnik GmbH). The samples (4Br2NIM: $C_3H_2BrN_3O_2$, AmBeed, 98% purity; 4Br5NIM: $C_3H_2BrN_3O_2$, AmBeed, 97% purity; 2NIM: $C_3H_3N_3O_2$, Sigma-Aldrich, 98% purity) were introduced to the endstation using an in-vacuum crucible. The samples were heated up to 130 °C with an effusion cell to ensure a sufficient sample density in the interaction region while simultaneously avoiding thermal degradation. Throughout the experiment, the vacuum chamber pressure was between 3.1×10^{-7} and 2.4×10^{-6} mbar.

We have used photon energies of 110 eV, 330 eV and 440 eV for Br 3d, C 1s, and N 1s ionisation, respectively. The ionisation of aforementioned core orbitals mostly leads to dicationic states formed *via* Auger decay. In a coincident experiment, multiple particles originating from the same individual molecule are detected in a way that enables the determination of various interdependent properties. Here, we have employed photoelectron–photoion–photoion coincidence (PEPIPICO) spectroscopy.

The experimental setup is presented in Fig. 2. The molecular sample jet from a crucible crossed the monochromatized photon beam. A portion of the ejected photoelectrons passed through an electrostatic lens system into a modified Scienta R4000 hemispherical electron analyser, which is equipped with a fast 40 mm diameter microchannel plate (MCP) and a resistive anode position sensitive detector (Quantar Inc.). The pass energy of the electron analyser was set at 100 eV. Electron detection was used as a trigger for the pulsed ion extraction voltage U_S ($\pm$ 250 V) that was applied across the source region of a modified Wiley-McLaren ion time-of-flight TOF spectrometer.[23] After the initial acceleration, the ions passed through a focusing lens element with voltage U_L (−333 V) and were accelerated to their final velocities by the drift tube voltage U_A (−1483 V). The ion TOF spectrometer is equipped with an 80 mm MCP and HEX-anode detector (Roentdek).

Events recorded after photoelectron-triggered extraction pulses are a mixture of true and false electron-ion coincidences. Ergo, we have also extracted ions using "random" triggers, which were obtained from a pulse generator at a constant

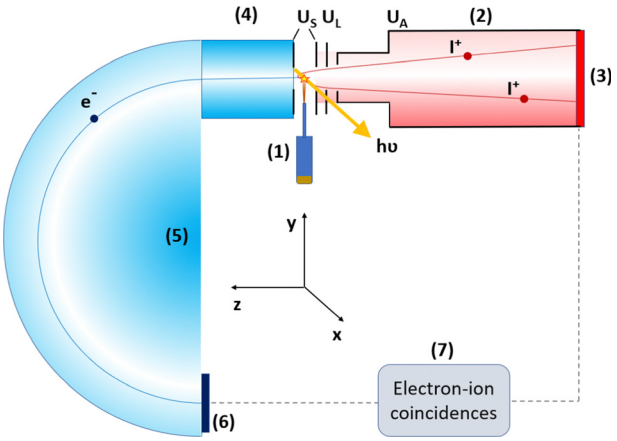

Fig. 2 Schematics of the used electron–ion coincidence setup. The main components are shown: (1) sample crucible and inlet, (2) ion TOF spectrometer, (3) ion detector, (4) electron lens, (5) electron analyser, (6) electron detector, and (7) data acquisition system. More details are given in Section 2.

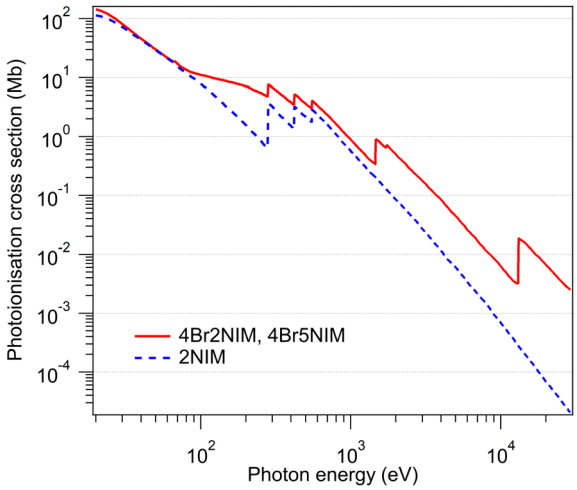

Fig. 3 Photoionisation cross-sections on a logarithmic scale for 4Br2NIM, 4Br5NIM, and 2NIM, approximated from atomic photoionisation cross sections.[26]

frequency. Events related to these random triggers can be thought of as consisting of purely false coincidences and they can be used to subtract a false coincidence background. The concepts of false coincidences, random triggers and background removal are explained in detail elsewhere.[24,25]

The experimental environment contained some trace impurities. Fortunately, the samples and the contamination were clearly distinguishable from one another in the photoelectron spectra. Therefore, we were able to filter out the coincident events due to the contamination from the data.

3 Radiosensitizing effects of heavy-element substitution

Substituting a hydrogen atom with bromine increases both the photoabsorption and the electron impact ionisation cross-sections. In Fig. 3 we present the photoabsorption cross-sections approximated from atomic data.[26] The enhancement in the cross section by bromination varies with photon energy, but becomes very significant, even over two orders of magnitude, after surpassing the Br 1s photoionisation edge at approximately 13 keV. Ergo, the most drastic increase occurs in the X-ray region for superficial and orthovoltage radiotherapy, which are used in the treatment of *e.g.* skin cancer. As the molecules have no deeper core orbitals, the cross section will then decrease at even higher photon energies.

Fig. 4 in turn shows ionisation cross-sections by electron impact, which were calculated using the Binary–Encounter–Bethe (BEB) model.[27] The necessary orbital constants (binding energy, average orbital kinetic energy, occupation number) were from Hartree–Fock simulations (aug-cc-pVDZ basis set[28,29] on version 5.0.2 of ORCA[30–32]) and we approximated the dipole constant in the BEB model to be 1 for each orbital. At 30 eV electron kinetic energy, the electron impact ionisation cross-section of 4Br2NIM is increased by a ratio of 1.13 with

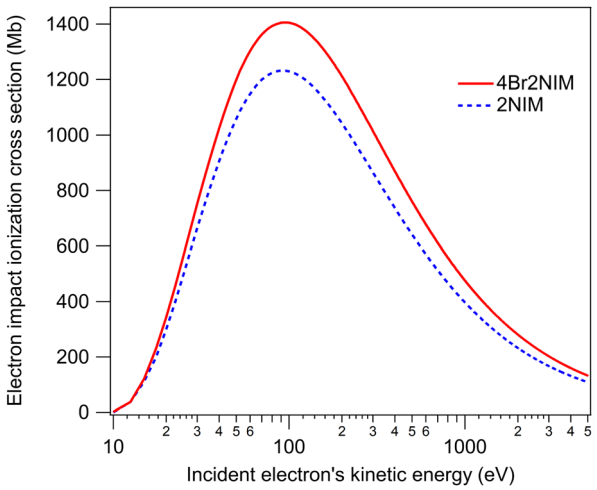

Fig. 4 Approximated ionisation cross-sections upon electron collision as a function of incident electron's kinetic energy.

respect to that of 2NIM. This ratio increases slowly as the energy increases, reaching a value of ≈1.22 by 5 keV. The largest contributions to the total cross section in the calculation come from valence orbitals. Bromination increases the number of valence electrons by a factor of 1.14 (from 42 to 48, while the total number of electrons is increased from 58 to 92), which closely reflects the ratio by which the approximated electron impact cross-section increases.

After 4Br2NIM or 4Br5NIM dissociates, the bromine atom will end up either in a neutral or a charged fragment. We do not know what kind of radiosensitizing capabilities these bromine-containing fragments may or may not possess. However, as both the Br radical and Br^+ cation are highly reactive species, we expect them to be detrimental to (cancerous) cells. This study will also consider the combined release of various active (or potentially active) radicals and ions. For example, if

bromination of a nitroimidazole molecule results in a fragmentation landscape with a strongly inhibited NO or NO+ release, the net radiosensitizating effect might not be improved at all.

4 Results and discussion

4.1 Analysis

We present the results of the three-particle PEPIPICO measurements in three different forms as TOF spectra, photoelectron spectra and two-dimensional PIPICO maps. A representative TOF spectrum and a PIPICO map from the C 1s PEPIPICO experiment of 4Br2NIM are illustrated in Fig. 5 and 6, while the corresponding graphs for the other two samples are included in the ESI.† The TOF spectra were mainly used to identify the detected ionic fragments and the photoelectron spectra were used as a filter to select specific coincident ion pairs for the analysis. A PIPICO map is a way to present these coincident ion pairs. The flight times of the two ions are plotted against each other, with the faster ion on the X-axis and the slower one on the Y-axis. The map is a 2D histogram, and here the number of ion pairs within a 2D bin is colour-coded.

Based on the flight times of identified fragments we defined rectangular regions of interest (ROI) in the PIPICO maps at locations, where true coincident ion pairs could appear. The ROI dimensions and orientations were manually optimised to match the observed patterns. In some cases neighbouring ion pairs overlap, making the underlying individual patterns indistinguishable. In these cases, we opted to combine the individual ROIs into one to avoid selecting ROIs arbitrarily.

From each of the ROIs we obtained the number of detected ion pairs for both the electron triggers and the random triggers. Subtracting the latter from the former after normalization gives us, on average, the number of true coincident ion pairs per trigger. During the analysis, we filtered out ROIs where the standard error for the true coincident ion pair counts was greater than 50%. By normalising the sum of all the remaining ion pairs per trigger to one, we obtain trigger-wise branching fractions for production of specific coincident ion pairs (or groups of pairs in the case of combined ROIs). Furthermore, by virtue of knowing the cations constituting each ion pair, it is straightforward to calculate branching fractions for specific ions.

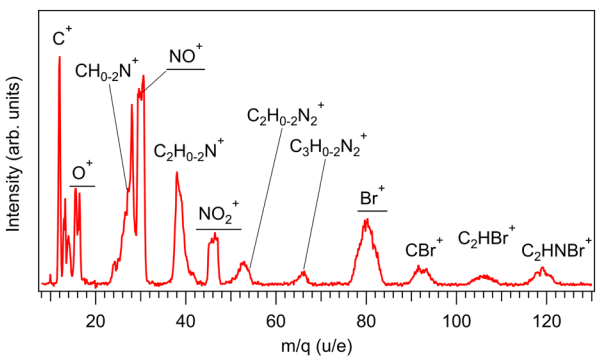

Fig. 5 A TOF spectrum from the C 1s PEPIPICO experiment of 4Br2NIM. A false coincidence background has been removed and flight times have been converted to mass-to-charge ratio scale. The fragments of the greatest interest have been underscored.

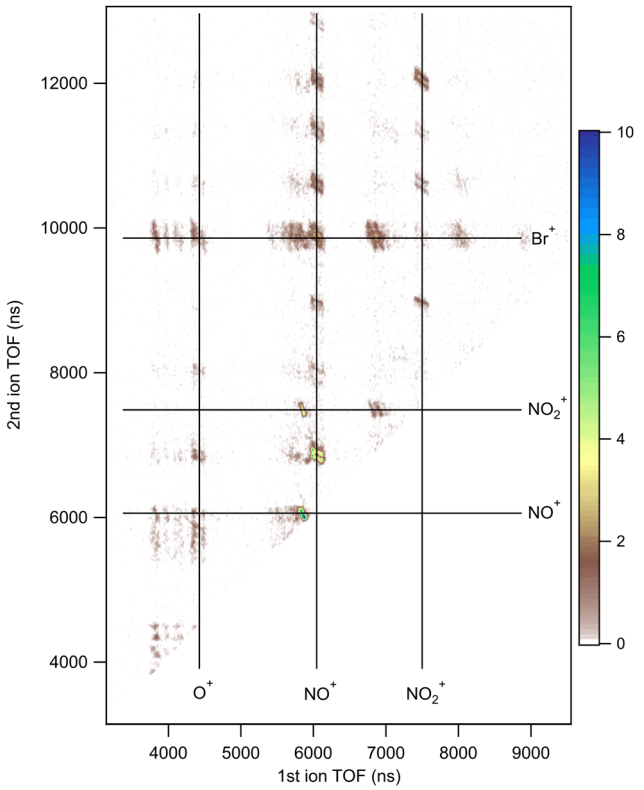

Fig. 6 PIPICO map of 4Br2NIM upon C 1s ionisation. Dissociation is characterized by the release of O^+, NO^+, NO_2^+, and Br^+. Ion pairs, which contain a bromine atom (2nd ion TOF > 9500 ns), form two adjacent patterns mostly due to the ^{79}Br and ^{81}Br isotopes that are found in approximately 1 : 1 ratio. For lighter ion pairs the possible adjacent patterns are a result of hydrogen loss.

Although in the present experiment we did not detect neutral species, their total atomic composition can be inferred from ionic fragments that were detected. Furthermore, separation of smaller neutral fragments is in some cases indicated by a careful analysis of the slopes of the PIPICO patterns (see, *e.g.*, ref. 33–35). Here, the data suggest that the release of neutral Br and NO_2 accompanies some of the PIPICO patterns.

As the release of neutral NO radicals cannot be resolved well here, nitrosonium NO^+ becomes the most interesting dissociation product in terms of radiosensitization. Both NO and NO^+ are capable of mediating damage to DNA *via* various pathways in cellular environment.[12,36,37] Additionally, NO^+ may recombine with an electron to form a NO radical. We also extend our focus on Br^+ and other ions related to the nitro group: NO_2^+ (radical, may dissociate further), O^+ (radical) and N^+. We note that nitrogen fragments may be obtained from both the nitro group and the imidazole ring.

4.2 Fragment branching fractions upon core ionisation

In Sections 4.2.1 and 4.2.2, we discuss the release of various charged fragments, concentrating on the ones with

radiotherapeutic relevance (N^+, O^+, NO^+, NO_2^+ and Br^+). Their branching fractions are presented in Table 1 per each studied atomic core orbital. For comparison between the samples, we have additionally tabulated the arithmetic mean over the core orbitals (from Br 3d, C 1s and N 1s entries). The table also lists the branching fractions per chemically inequivalent N 1s orbitals.

The two rightmost columns of table, SUM1 and SUM2, are composite values calculated from the single-ion branching fractions. SUM1 is the sum of the abundances of the NO^+, NO_2^+, N^+, and O^+ ions obtained by removing possible overlaps between the numbers. For instance, the ion pair of O^+ and NO^+ is included both in the O^+ and the NO^+ branching fraction, and thus it needs to be subtracted once in the calculation. In brief, SUM1 stands as an indicator of charge localization on the nitro group. Naturally, such a charge localization may result in a fragment not included in the calculation, but those cases are omitted from the analysis for simplicity. SUM2 is obtained in a similar manner but it adds Br^+ into the consideration, reflecting the likelihood that dicationic dissociation results in the release of at least one of the five aforementioned, presumably toxic ions.

4.2.1 Effects of bromination and the location of the nitro site. With both brominated samples regardless of the ionised atomic core orbital, the dicationic dissociation landscape is strongly characterized by release of Br^+, O^+, NO^+ and NO_2^+ (highlighted in Fig. 6). Especially, the release of NO^+ and Br^+ is notable. This is also evident in the TOF spectrum of Fig. 5. The two highest peaks in the spectrum belong to C^+ and NO^+, but C^+ is very narrow having an area under the curve much smaller than that of NO^+. The peaks assigned to the Br-containing fragments are rather broad, which can be attributed, among other things, to the ^{79}Br and ^{81}Br isotopes that are found in approximately 1 : 1 ratio. We can also note two asymmetric structures on both sides of the NO^+ peak, corresponding to masses at approximately 24–28 u and 38–42 u. They can be associated with several different fragments that require breaking of the imidazole ring.

The NO_2^+, NO^+, and O^+ fragments necessitate charge localization to the nitro group. Such a process could also yield N^+ ions. However, each sample molecule contains three nitrogen atoms, one in the nitro group and two in the ring, and there is no way to identify which nitrogen atom we have detected. Therefore, charge localization to the nitro group is not a strict prerequisite for the detection of nitrogen cations and as a result the N^+ branching fractions likely reflect the described charge localization only partially (in future experiments this could be resolved by using an isotope-substituted molecule with an ^{15}N atom in the nitro group). However, pathways leading to the release of N^+ are not very prominent, so the effect of this uncertainty on the overall picture is not significant.

Generally, the branching fractions obtained upon ionising different core orbitals of the same molecule are within a few percentage points from one another. Consequently, the mean branching fraction covering all core ionisation sites of a sample offers a reasonable way of comparing the samples. From the viewpoint of radiotherapeutic application, averaging over all possible core-ionisation sites represents fairly well the ionising

Table 1 Single ion branching fractions (%) coincident with selected photoelectrons presented for studied samples. SUM1 is the combined branching fraction of ion pairs containing at least one ion that originates from the nitro group. SUM2 is the combined branching fraction for pairs with at least one ion being of the nitro group origin or Br^+. Parameters SUM1 and SUM2 remove the effect of double counting certain events (*e.g.* ion pair (NO^+, Br^+) is included both in the NO^+ and Br^+ columns, and needs to be subtracted from the calculation once). $-NO_2$, –N(–H)– and –N═ refer to the N 1s peaks (Fig. 8) while the N 1s entry is the arithmetic mean of the three

Sample	Photoelectron	NO^+	NO_2^+	N^+	O^+	Br^+	SUM1	SUM2
4Br2NIM	Br 3d	38.1 ± 0.6	10.7 ± 0.3	2.6 ± 0.2	13.0 ± 0.4	35.0 ± 0.6	62.5 ± 0.7	85.9 ± 0.8
	C 1s	37.6 ± 0.4	12.6 ± 0.3	3.8 ± 0.2	11.5 ± 0.3	34.0 ± 0.5	63.8 ± 0.5	86.6 ± 0.6
	N 1s	39.4 ± 1.0	9.3 ± 0.5	3.9 ± 0.4	14.5 ± 0.7	38.5 ± 1.2	65.1 ± 1.4	90.8 ± 1.6
	Mean	**38.4 ± 0.7**	**10.9 ± 0.4**	**3.4 ± 0.3**	**13.0 ± 0.5**	**35.8 ± 0.8**	**63.8 ± 0.9**	**87.8 ± 1.1**
	N 1s, $-NO_2$	35.3 ± 1.3	0.8 ± 0.3	5.4 ± 0.5	21.2 ± 1.0	44.5 ± 1.2	60.0 ± 1.6	90.2 ± 2.0
	N 1s, –N(–H)-	39.8 ± 0.7	7.6 ± 0.4	3.9 ± 0.3	12.9 ± 0.5	39.0 ± 0.8	62.3 ± 0.9	88.6 ± 1.1
	N 1s, –N═	43.2 ± 1.1	19.5 ± 0.7	2.2 ± 0.3	9.3 ± 0.6	32.0 ± 1.4	73.0 ± 1.4	93.5 ± 1.6
4Br5NIM	Br 3d	33.5 ± 0.5	9.9 ± 0.3	2.5 ± 0.2	12.0 ± 0.3	42.3 ± 0.5	56.4 ± 0.7	88.0 ± 0.8
	C 1s	35.9 ± 0.5	11.0 ± 0.3	3.6 ± 0.2	11.0 ± 0.3	38.3 ± 0.5	59.8 ± 0.6	88.8 ± 0.7
	N 1s	36.4 ± 1.1	8.0 ± 0.5	5.0 ± 0.5	14.7 ± 0.8	38.5 ± 1.2	61.5 ± 1.5	89.9 ± 1.8
	Mean	**35.3 ± 0.8**	**9.6 ± 0.4**	**3.7 ± 0.3**	**12.6 ± 0.5**	**39.7 ± 0.8**	**59.2 ± 1.0**	**88.9 ± 1.2**
	N 1s, $-NO_2$	32.9 ± 1.5	0.2 ± 0.1	7.2 ± 0.7	21.6 ± 1.1	44.2 ± 1.4	57.5 ± 1.9	90.5 ± 2.5
	N 1s, –N(–H)–	36.7 ± 0.7	6.9 ± 0.4	4.4 ± 0.3	12.0 ± 0.5	39.1 ± 0.8	58.1 ± 0.9	87.5 ± 1.2
	N 1s, –N═	39.7 ± 1.0	16.9 ± 0.7	3.3 ± 0.4	10.4 ± 0.6	32.1 ± 1.3	68.9 ± 1.4	91.6 ± 1.6
2NIM	C 1s	47.2 ± 0.4	14.7 ± 0.3	4.6 ± 0.2	12.5 ± 0.2		76.3 ± 0.5	
	N 1s	43.1 ± 0.7	12.7 ± 0.4	5.8 ± 0.3	16.1 ± 0.5		74.4 ± 1.0	
	Mean	**45.1 ± 0.6**	**13.7 ± 0.3**	**5.2 ± 0.3**	**14.3 ± 0.4**		**75.3 ± 0.8**	
	N 1s, $-NO_2$	40.4 ± 0.9	2.9 ± 0.3	7.5 ± 0.4	23.0 ± 0.7		69.9 ± 1.2	
	N 1s, –N(–H)–	45.4 ± 0.6	11.6 ± 0.3	5.6 ± 0.2	14.1 ± 0.3		73.5 ± 0.7	
	N 1s, –N═	43.5 ± 0.7	23.5 ± 0.5	4.3 ± 0.3	11.3 ± 0.4		79.7 ± 0.9	

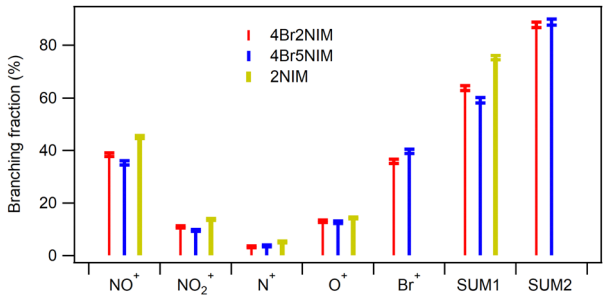

Fig. 7 Comparison of mean branching fractions (over studied core-ionisation cases) between sample molecules. Overall, the observed differences between the brominated samples are minor.

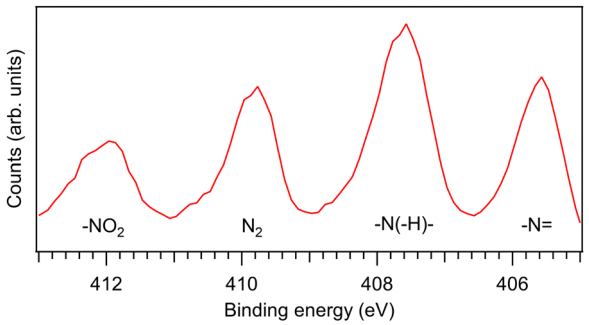

Fig. 8 The N 1s coincident electron spectrum of 4Br2NIM. The second peak from the left belongs to rest gas (N_2), the remaining three peaks correspond to the chemically inequivalent nitrogen atoms in the sample (see assignments).

effect of medical X-rays that are generally of much higher energy than the orbitals considered here and therefore not site-selective in absorption.

Fig. 7 presents a graphical comparison between the sample molecules using the mean branching fraction values from Table 1. We note that the differences between 4Br2NIM and 4Br5NIM are minor. 4Br2NIM exhibits a slightly more charge localization to the nitro group (SUM1) than 4Br5NIM, which in turn showcases slightly more Br^+ release. All in all, approximately nine out of ten dicationic dissociation events lead to release of potentially radiosensitizing cation (SUM2) with both brominated samples. Comparison to 2NIM reveals that bromination does inhibit charge localization to the nitro group but the effect is not drastic (SUM1 from 75.3% to 63.8% and to 59.2% for 4Br2NIM and 4Br5NIM respectively). This is a small yet important remark for the potential viability of halogenation of nitroimidazoles. An earlier study with dicationic 4(5)-nitroimidazole and 1-methyl-5-nitroimidazole, a poor radiosensitizer, showed that methylation greatly suppressed both charge localization to the nitro group (reduced by approximately two thirds) and NO/NO^+ production (reduced by approximately nine tenths).[5,7] Taking into account the increased ionisation cross-sections, possibility of Auger cascades and the high yield of potentially harmful ionic fragments upon core ionisation, we conclude that the option of halogenating nitroimidazoles to produce new radiosensitizer candidates seems promising from the photodissociation point of view.

4.2.2 Ionisation-site-dependent effects. In Table 1 we have included N 1s entries for the three chemically inequivalent nitrogen atoms (–N═, –N(–H)– and $–NO_2$). Since the N 1s photoelectron peaks (Fig. 8) are well separated in all samples, coincident events can be filtered based on which N 1s site was ionised. The photoelectron lines were identified *via* simulation (Hartree–Fock, aug-cc-pVDZ,[28,29] version 5.0.2 of ORCA[30–32]) and confirmed against literature on nitroimidazoles.[38] The spectrum also contains a fourth peak, which originates from the residual N_2 molecules in the vacuum chamber. An analogous site-selective study cannot be done with the carbon atoms, as the photoelectron peaks originating from different sites are overlapping, and therefore only a single entry is given.

The three photoelectron lines from the sample in Fig. 8 have different intensities. Since the measurement was done using a fixed kinetic energy window, we attribute this largely to instrumental effects such as the different transmission of the hemispherical analyser for electrons arriving at the detector at different radii as well as variations of the detector's sensitivity across its area. Some deviation from a 1:1:1 intensity ratio might also be expected due to inelastic scattering of outgoing photoelectrons.[39] The simple N 1s entry in the Table 1 is not determined from a combined coincidence data covering all N 1s photoelectron lines. Rather, it is the arithmetic mean of the three aforementioned entries. In the former case, individual core-ionisation sites would be given different weights according to the corresponding photoelectron line intensity; now they are all given equal weights and we thus eliminate the instrumental effects mentioned earlier and the dependence of the cross-section on the chemical environment.

Ionisation site dependency of the ensuing fragmentation has less importance *vis-à-vis* the radiosensitizing properties, but is significant for deeper understanding of the X-ray induced dynamics and its theoretical modeling. Considering how similar the Br 3d, C 1s and N 1s (mean) related branching fractions are, the branching fractions differ a lot when ionising different nitrogen atoms. For example, with 4Br2NIM the branching fraction of NO_2^+ experiences an approximately twentyfold increase (from 0.8 ± 0.3% to 19.5 ± 0.7%) when the –N═ nitrogen site is ionised instead of the $–NO_2$ site. A closer inspection reveals a recurring general trend: ionisation of –N═ and $–NO_2$ sites results in the extreme values for the NO^+, NO_2^+, N^+, O^+ and Br^+ single ion branching fractions in the Table 1, while –N(–H)– is the middle entry of the three. Only NO^+ with 2NIM breaks the pattern.

The irradiated cellular environment will contain free electrons and, consequently, some radiosensitizer molecules will undergo valence ionisation and the ensuing dissociation is naturally very different from the dicationic dissociation. In addition to the coincidence measurements upon core ionisation, we ran non-coincident ion TOF measurements upon valence ionisation using a photon energy of 30 eV. Yet the measurements contained impurities, which could not be

reliably removed during analysis as with the coincidence data, barring us from in-depth quantitative analysis. However, as a general overview regarding the aforementioned fragments of interest, we detected notable release of NO^+ – but no Br^+ – with each sample. Additionally, we saw evidence of NO release especially from 2NIM and 4Br2NIM. The TOF spectra upon valence ionisation have been included in the ESI.†

5 Conclusions

Photodissociation of brominated nitroimidazoles 4Br2NIM and 4Br5NIM upon core ionisation (Br 3d, C 1s or N 1s) leads to notable release of Br^+, O^+, NO^+ and NO_2^+. This is a promising sign for radiosensitization applications because the release of nitro-related fragments have generally been linked to radiosensitizing capabilities of nitroimidazoles. Comparison to non-brominated 2NIM reveals that bromination slightly inhibits charge localization to the nitro group. Yet, with the release of likely harmful Br^+, approximately 90% of dicationic dissociation events produce ions that may damage cancerous cells. Bromination of nitroimidazoles also increases the likelihood of the molecule being ionised by a given radiation dose. Moreover, the possibility of Auger cascades leads to a higher rate of secondary ionisations and, generally, a localised energy deposition in the vicinity of the molecule. Based on this photodissociation study, we conclude that brominated nitroimidazoles appear to be a promising avenue for research towards multifunctional radiosensitizers, even if the clinical usability of the sample molecules studied here remains to be investigated. Future research ought to be extended to other halogen elements, other nitroimidazole compounds and to clinical studies.

From a more fundamental point of view relevant to, *e.g.*, molecular dynamics modeling, we observed very significant ionisation-site-dependent effects on the fragmentation patterns at the N K-edge. The selection of a specific nitrogen atom as the core-ionisation site was noted to influence the production of the NO_2+ fragment in particular, but also that of other fragments. These effects are more surprising in the light of overall similarity of the fragmentation patterns, when comparing core-ionisation of different elements in a molecule as averages over different chemical sites of the same element.

Conflicts of interest

There are no conflicts to declare.

Acknowledgements

LP acknowledges financial support from the Vilho, Yrjö and Kalle Väisälä Foundation, the Turku University Foundation and the EXACTUS doctoral programme of the University of Turku Graduate School. MB acknowledges the Estonian Research Council grant (MOBTP1013) for the financial support and the Centre of Excellence ''Advanced Materials and High-technology Devices for Sustainable Energetics, Sensorics, and Nanoelectronics'' TK141. JN and AV acknowledge the Academy of Finland for funding *via* project 331234. KK acknowledges the Estonian Research Council (grant PRG551) and the European Regional Development Fund (project MOBTT42) under the Mobilitas Pluss programme for the support. PEJ acknowledges support from the Swedish Research Council. EK acknowledges funding by the Academy of Finland (project 295551). We acknowledge MAX IV Laboratory for time on the FinEstBeAMS beamline under proposal 20200355 and the help of the beamline staff during the experiment. Research conducted at MAX IV, a Swedish national user facility, is supported by the Swedish Research council under contract 2018-07152, the Swedish Governmental Agency for Innovation Systems under contract 2018-04969, and Formas under contract 2019-02496.

Notes and references

1 K. Kobayashi, N. Usami, E. Porcel, S. Lacombe and C. Le Sech, *Mutat. Res., Rev. Mutat. Res.*, 2010, **704**, 123–131.
2 B. T. Oronsky, S. J. Knox and J. Scicinski, *Transl. Oncol.*, 2011, **4**, 189–198.
3 H. Wang, X. Mu, H. He and X.-D. Zhang, *Trends Pharmacol. Sci.*, 2018, **39**, 24–48.
4 L. Gong, Y. Zhang, C. Liu, M. Zhang and S. Han, *Int. J. Nanomed.*, 2021, **16**, 1083.
5 E. Itälä, K. Tanzer, S. Granroth, K. Kooser, S. Denifl and E. Kukk, *J. Mass Spectrom.*, 2017, **52**, 770–776.
6 A. Cartoni, A. Casavola, P. Bolognesi, M. Castrovilli, D. Catone, J. Chiarinelli, R. Richter and L. Avaldi, *J. Phys. Chem. A*, 2018, **122**, 4031–4041.
7 E. Itälä, H. Myllynen, J. Niskanen, J. González-Vázquez, Y. Wang, D. T. Ha, S. Denifl and E. Kukk, *J. Phys. Chem. A*, 2019, **123**, 3074–3079.
8 P. Bolognesi, V. Carravetta, L. Sementa, G. Barcaro, S. Monti, P. M. Mishra, A. Cartoni, M. C. Castrovilli, J. Chiarinelli, S. Tosic, B. P. Marinkovic, R. Richter and L. Avaldi, *Front. Chem.*, 2019, **7**, 151.
9 R. Meißner, L. Feketeová, A. Ribar, K. Fink, P. Limão-Vieira and S. Denifl, *J. Am. Soc. Mass Spectrom.*, 2019, **30**, 2678–2691.
10 E. Itälä, J. Niskanen, L. Pihlava and E. Kukk, *J. Phys. Chem. A*, 2020, **124**, 5555–5562.
11 M. Satta, A. R. Casavola, A. Cartoni, M. C. Castrovilli, D. Catone, J. Chiarinelli, S. Borocci, L. Avaldi and P. Bolognesi, *ChemPhysChem*, 2021, **22**, 2387–2391.
12 B. T. Oronsky, S. J. Knox and J. J. Scicinski, *Transl. Oncol.*, 2012, **5**, 66–71.
13 W. Krause, A. Jordan, R. Scholz and J.-L. M. Jimenez, *Anticancer Res.*, 2005, **25**, 2145–2151.
14 J. M. Brown, *Int. J. Radiat. Oncol., Biol., Phys.*, 1984, **10**, 425–429.
15 E. Itälä, D. T. Ha, K. Kooser, E. Rachlew, M. A. Huels and E. Kukk, *J. Chem. Phys.*, 2010, **133**, 10B614.

16 M. C. Castrovilli, P. Bolognesi, A. Cartoni, D. Catone, P. OKeeffe, A. R. Casavola, S. Turchini, N. Zema and L. Avaldi, *J. Am. Soc. Mass Spectrom.*, 2014, **25**, 351–367.
17 S. Makurat, P. Spisz, W. Kozak, J. Rak and M. Zdrowowicz, *Int. J. Mol. Sci.*, 2019, **20**, 1308.
18 P. Spisz, M. Zdrowowicz, S. Makurat, W. Kozak, K. Skotnicki, K. Bobrowski and J. Rak, *Molecules*, 2019, **24**, 2819.
19 M. R. Chowdhury, J. M. Monti, D. Misra, P. F. Weck, R. D. Rivarola and L. C. Tribedi, *New J. Phys.*, 2022, **24**, 073035.
20 K. Kooser, A. Kivimäki, P. Turunen, R. Pärna, L. Reisberg, M. Kirm, M. Valden, M. Huttula and E. Kukk, *J. Synchrotron Radiat.*, 2020, **27**, 1080–1091.
21 R. Pärna, R. Sankari, E. Kukk, E. Nõmmiste, M. Valden, M. Lastusaari, K. Kooser, K. Kokko, M. Hirsimäki, S. Urpelainen, P. Turunen, A. Kivimäki, V. Pankratov, L. Reisberg, F. Hennies, H. Tarawneh, R. Nyholm and M. Huttula, *Nucl. Instrum. Methods Phys. Res., Sect. A*, 2017, **859**, 83–89.
22 K. Chernenko, A. Kivimäki, R. Pärna, W. Wang, R. Sankari, M. Leandersson, H. Tarawneh, V. Pankratov, M. Kook, E. Kukk, L. Reisberg, S. Urpelainen, T. Käämbre, F. Siewert, G. Gwalt, A. Sokolov, S. Lemke, S. Alimov, J. Knedel, O. Kutz, T. Seliger, M. Valden, M. Hirsimäki, M. Kirm and M. Huttula, *J. Synchrotron Radiat.*, 2021, **28**, 1620–1630.
23 W. C. Wiley and I. H. McLaren, *Rev. Sci. Instrum.*, 1955, **26**, 1150–1157.
24 G. Prümper and K. Ueda, *Nucl. Instrum. Methods Phys. Res., Sect. A*, 2007, **574**, 350–362.
25 E. Itälä, D. Ha, K. Kooser, M. Huels, E. Rachlew, E. Nõmmiste, U. Joost and E. Kukk, *J. Electron Spectrosc. Relat. Phenom.*, 2011, **184**, 119–124.
26 B. L. Henke, E. M. Gullikson and J. C. Davis, *At. Data Nucl. Data Tables*, 1993, **54**, 181–342.
27 Y.-K. Kim and M. E. Rudd, *Phys. Rev. A: At., Mol., Opt. Phys.*, 1994, **50**, 3954.
28 T. H. Dunning, *J. Chem. Phys.*, 1989, **90**, 1007–1023.
29 A. K. Wilson, D. E. Woon, K. A. Peterson and T. H. Dunning, *J. Chem. Phys.*, 1999, **110**, 7667–7676.
30 F. Neese, *Wiley Interdiscip. Rev.: Comput. Mol. Sci.*, 2012, **2**, 73–78.
31 F. Neese, F. Wennmohs, U. Becker and C. Riplinger, *J. Chem. Phys.*, 2020, **152**, 224108.
32 F. Neese, *Wiley Interdiscip. Rev.: Comput. Mol. Sci.*, 2022, **12**, e1606.
33 A. Santos, C. Lucas and G. de Souza, *Chem. Phys.*, 2002, **282**, 315–326.
34 H. Levola, E. Itälä, K. Schlesier, K. Kooser, S. Laine, J. Laksman, D. T. Ha, E. Rachlew, M. Tarkanovskaja, K. Tanzer and E. Kukk, *Phys. Rev. A: At., Mol., Opt. Phys.*, 2015, **92**, 063409.
35 L. Pihlava, J. Niskanen, K. Kooser, C. Stråhlman, S. Maclot, A. Kivimäki and E. Kukk, *Phys. Chem. Chem. Phys.*, 2021, **23**, 21249–21261.
36 T. Turney and G. Wright, *Chem. Rev.*, 1959, **59**, 497–513.
37 S. Burney, J. L. Caulfield, J. C. Niles, J. S. Wishnok and S. R. Tannenbaum, *Mutat. Res., Fundam. Mol. Mech. Mutagen.*, 1999, **424**, 37–49.
38 L. Feketeova, O. Plekan, M. Goonewardane, M. Ahmed, A. L. Albright, J. White, R. A. OHair, M. R. Horsman, F. Wang and K. C. Prince, *J. Phys. Chem. A*, 2015, **119**, 9986–9995.
39 J. Söderström, N. Mårtensson, O. Travnikova, M. Patanen, C. Miron, L. Sæthre, K. J. Børve, J. J. Rehr, J. J. Kas, F. D. Vila, T. D. Thomas and S. Svensson, *Phys. Rev. Lett.*, 2012, **108**, 193005.